



Article

Optimizing Economy with Comfort in Climate Control System Scheduling for Indoor Ice Sports Venues' Spectator Zones Considering Demand Response

Zhuoqun Du, Yisheng Liu, Yuyan Xue * and Boyang Liu 🗅

School of Economics and Management, Beijing Jiaotong University, Beijing 100044, China; qzdu7551@bjtu.edu.cn (Z.D.); yshliu1@bjtu.edu.cn (Y.L.); 20113060@bjtu.edu.cn (B.L.) * Correspondence: 23120654@bjtu.edu.cn

Abstract

With the growing popularity of ice sports, indoor ice sports venues are drawing an increasing number of spectators. Maintaining comfort in spectator zones presents a significant challenge for the operational scheduling of climate control systems, which integrate ventilation, heating, and dehumidification functions. To explore economic cost potential while ensuring user comfort, this study proposes a demand response-integrated optimization model for climate control systems. To enhance the model's practicality and decision-making efficiency, a two-stage optimization method combining multi-objective optimization algorithms with the technique for order preference by similarity to an ideal solution (TOPSIS) is proposed. In terms of algorithm comparison, the performance of three typical multiobjective optimization algorithms—NSGA-II, standard MOEA/D, and Multi-Objective Brown Bear Optimization (MOBBO)—is systematically evaluated. The results show that NSGA-II demonstrates the best overall performance based on evaluation metrics including runtime, HV, and IGD. Simulations conducted in China's cold regions show that, under comparable comfort levels, schedules incorporating dynamic tariffs are significantly more economically efficient than those that do not. They reduce operating costs by 25.3%, 24.4%, and 18.7% on typical summer, transitional, and winter days, respectively. Compared to single-objective optimization approaches that focus solely on either comfort enhancement or cost reduction, the proposed multi-objective model achieves a better balance between user comfort and economic performance. This study not only provides an efficient and sustainable solution for climate control scheduling in energy-intensive buildings such as ice sports venues but also offers a valuable methodological reference for energy management and optimization in similar settings.

Keywords: climate control systems; economic cost; thermal comfort; optimization; indoor ice sports venues; demand response



Academic Editors: Frank Werner and Vahid Kayvanfar

Received: 5 June 2025 Revised: 14 July 2025 Accepted: 18 July 2025 Published: 20 July 2025

Citation: Du, Z.; Liu, Y.; Xue, Y.; Liu, B. Optimizing Economy with Comfort in Climate Control System Scheduling for Indoor Ice Sports Venues' Spectator Zones Considering Demand Response. *Algorithms* **2025**, *18*, 446. https://doi.org/10.3390/a18070446

Copyright: © 2025 by the authors. Licensee MDPI, Basel, Switzerland. This article is an open access article distributed under the terms and conditions of the Creative Commons Attribution (CC BY) license (https://creativecommons.org/licenses/by/4.0/).

1. Introduction

Ice sports venues have become an integral part of people's lives as places for public fitness, professional training, and competitions. Due to their unique functional attributes, ice sports venues have stringent requirements for the ice surface and the surrounding thermal and humidity environments, which are often maintained through climate systems [1,2]. Owing to the complex and large-scale structure of ice sports venues, their indoor temperature and humidity are influenced by a wide range of factors. In addition, the spatial

divisions within the venue are complex, including the near-ice space, the athlete competition areas, and the spectator areas, all of which are interconnected, and there are significant differences in the thermal and humidity conditions across these different spaces [3,4]. To meet the above requirements, the climate control system consists of 2–3 sets of independent cold and heat source systems, which are used for ice refrigeration and dehumidification of the ice zone and spectator zones. Specifically, the climate control system of ice sports venues is composed of equipment such as ice-making units, dehumidification units, and air conditioning units. The ice-making units maintain ice surface temperature control requirements and ensure temperature uniformity through the circulation of appropriate coolants or refrigerants. Dehumidification units, working in conjunction with supply and return air terminals, regulate humidity parameters in the ice rink area to ensure that air humidity meets the demand [5]. When auxiliary areas such as spectator stands are present, ventilation systems with cooling functions and radiant heaters are typically installed to ensure essential thermal environmental conditions [6]. Due to differences in temperature and humidity requirements and influencing factors between the ice surface and its surrounding areas and the spectator stands in ice sports venues, inadequate temperature and humidity control in the spectator area can negatively impact the audience experience. This, in turn, may reduce venue attendance and further affect ticket revenue. However, operating at full capacity also increases energy costs. Therefore, the regulation of the thermal and humidity environment in the spectator area is crucial. For this reason, this study focuses on the climate control of spectator stands in ice sports venues.

The operation of the climate control system is a crucial component of ice sports venues [3]. This process also consumes a large amount of energy, resulting in high operating costs [7]. Therefore, it is of great significance to reasonably optimize the operation scheduling of the climate control system of the ice sports venues to reduce energy consumption, save costs, and promote stabilization of the indoor thermal and humidity environment.

In the optimization problem for the climate control system, the regulation strategies have shifted from proposing operational plans based on traditional standard conditions to dynamically and predictively formulating operational strategies. Deori considered uncertainty in building occupancy [8], Rupali Jain considered uncertainty in electricity prices, weather variations, and spectators in the room [9], Zhang considered occupancy data and weather forecast data, and Bozchalui considered dynamic electricity prices [10,11]. Rahim et al. proposed an innovative approach that integrates green roofs with atriums, demonstrating significant energy-saving effects during both winter and summer operations. It can be seen that the dynamic changes in electricity prices have become one of the important considerations in predictive control [12]. As an option for peak load management, demand response enables end users to manually or automatically reduce and shift their energy consumption, achieving the goal of cost reduction [13–16]. It also helps energy suppliers adjust load distribution to reduce peak demand and avoid exposing their infrastructure to critical stress [17]. Since predictive control strategies help match supply and demand, save energy, and reduce energy costs, this study considers dynamic electricity information, weather variation information, and audience presence information. This approach contributes to reasonably formulating the operational scheme for the climate control system in the spectator stands.

In the field of equipment system operation research, studies can be classified into single-objective and multi-objective approaches based on the number of optimization goals. In single-objective research, Zahedi studied a CCHP system coupled with a thermal energy storage tank, aiming to minimize the overall cost of fuel consumption, electricity purchase, electricity sale revenue, and system operation [18]. Siroky investigated intermittently heated radiant floor heating systems and proposed predictive control strategies, resulting

Algorithms 2025, 18, 446 3 of 28

in 10–12% energy savings during cold winter months compared to conventional control approaches [19]. Gwerder studied the energy-saving effects of predictive Integrated Room Automation (IRA), which maximizes the use of low-energy-cost actuators to maintain comfort within the desired range while minimizing energy consumption [20]. Nagpal proposed a co-optimization framework for minimizing energy costs and investigated the climate control of buildings utilizing a shared set of heat pumps through economic model predictive control [21]. Rupali Jain aimed to minimize electricity costs and discussed equipment start–stop strategies under both real-time and fixed pricing schemes. The results showed that shifting the operation of climate control equipment to periods of low electricity prices can lead to significant cost savings [9]. In summary, the majority of studies focus primarily on reducing energy consumption and minimizing energy costs as separate objectives.

In the multi-objective optimization research, Zhang aimed to achieve two objectives: minimizing energy consumption and stabilizing indoor temperature. To accomplish these goals, he proposed a model predictive control-based optimal temperature controller for air conditioning and mechanical ventilation systems in buildings [10]. Imandoust et al. also investigated a similar solar-driven MED system, aiming to maximize net profit and enhance unit production economy through system configuration optimization [22].

The thermal and humidity conditions in ice sports venues are complex, yet relatively little consideration has been given to the development of equipment operation strategies. Current research primarily focuses on operational strategies for ice sports venues from a single-objective perspective, without considering them from a multi-objective approach [9]. Given that the stands accommodate a substantial number of spectators, ensuring occupant comfort has become a primary objective. Additionally, cost and comfort are mutually constraining goals. Therefore, this study takes spectator comfort and energy cost as its objectives to achieve efficient and economical system operation. Furthermore, in the current research on climate control systems for ice sports venues, most studies focus on minimizing electrical energy costs, typically by optimizing the switching states of the climate control system equipment. However, these studies often overlook other important factors such as equipment startup and shutdown costs, operation and maintenance costs, and environmental impact costs. Therefore, while some progress has been made in optimizing energy costs, these studies fail to comprehensively reflect the overall benefits of the system.

The core of multi-objective optimization methods lies in providing a moderate number of Pareto solution sets of good quality within a limited computational time to support the solution of complex decision problems. Evolutionary algorithms have been widely used in the field of multi-objective optimization due to their superior search capability and low computational burden [23]. Among them, the Non-dominated Sorting Genetic Algorithm (NSGA-II), as a classical benchmark algorithm, combines the genetic algorithm with the non-dominated sorting mechanism and is able to search the global Pareto frontier efficiently, especially in large-scale problems, and has been proven to have a significant computational advantage over commercial optimization tools. In addition, the standard MOEA/D algorithm decomposes the multi-objective problem into multiple sub-problems through weight vectors and utilizes the neighborhood structure and Tchebycheff aggregation method to achieve a rigorous optimization process based on decomposition and neighborhood, which is suitable for scenarios with obvious objective conflicts and clear problem structure [24]. In recent years, MOBBO (Multi-Objective Brown Bear Optimization), as an emerging group intelligence algorithm, integrates the mechanisms of non-dominated sorting, external solution archiving, and brown bear foraging behavior and takes into account the ability of local exploitation and global exploration, which has shown strong performance advantages in high-dimensional and complex multi-objective engineering problems [25].

Algorithms 2025, 18, 446 4 of 28

Based on the above algorithms, three representative multi-objective optimization algorithms, NSGA-II, MOEA/D, and MOBBO, are selected for comparative analysis to systematically evaluate their applicability and differences in multi-objective scheduling problems. These three algorithms have their own characteristics in terms of optimization mechanism, search strategy, and solution set characteristics, which can comprehensively cover the mainstream technical paths in multi-objective optimization, have strong representativeness and complementarity, and provide multi-dimensional technical support for the solution of the multi-objective scheduling model in this study.

However, multi-objective optimization algorithms usually generate a large number of candidate solutions while providing high-quality solution sets, which may lead to decision-making difficulties. For this reason, this study further introduces the TOPSIS method [26], which assists the decision-making in selecting the optimal solution by calculating the distances between each solution in the solution set and the ideal solution. The multi-objective optimization algorithm fully ensures the diversity and global nature of the solution set, while the TOPSIS method introduces an objective sorting logic in the solution set. The two-stage optimization method improves the efficiency and practicability of optimal solution selection. The synergistic mechanism of "diversified search + rational decision-making" not only reduces the subjective intervention of manpower but also improves the operability and relevance of the solution, which demonstrates the outstanding comprehensive advantages in complex engineering optimization problems.

The innovations of this work are as follows:

- This study systematically integrates electricity, equipment start/stop, maintenance, and environmental costs for the first time, moving beyond the traditional focus on energy costs to achieve a more comprehensive optimization that considers equipment lifespan and environmental impact.
- An innovative approach combining multi-objective optimization with TOPSIS decision analysis is proposed, following a "search first, decide later" strategy. This greatly enhances the model's practicality and decision-making efficiency while incorporating demand-side analysis.
- This study systematically compares three algorithms—NSGA-II, MOEA/D, and MOBBO—assessing their suitability for ice rink climate control. It identifies the optimal algorithm and introduces a demand-side response strategy under time-of-use tariffs to reduce costs through load shifting and improve energy efficiency.

The remainder of this paper is organized as follows: Section 2 develops an approximate physical model of the ice sports venue for the multi-objective optimization of its climate control system. Section 3 presents a case study that compares three multi-objective optimization algorithms, identifies the most suitable one, and analyzes the optimization results based on the selected method. Section 4 provides discussion, and Section 5 concludes the paper.

2. Optimization Model

This study adopts a representative facility layout of an ice sports venue as the architectural model, as developed in prior research [27]. The specific equipment layout is shown in Figure 1 below.

This study focuses on the spectator stands of an ice sports venue. The climate control system in this area comprises a ventilation system, a radiant heating system, and a dehumidifier. The ventilation unit provides fresh air while also delivering air at a regulated temperature to help maintain thermal comfort in the spectator area. Meanwhile, the radiant heaters assist with space heating, and the independent dehumidification system is responsible for maintaining appropriate humidity levels. To ensure coordinated operation among

Algorithms **2025**, 18, 446 5 of 28

these subsystems, an optimization model for operational strategy is developed, which intelligently generates control commands based on the current system status to regulate device operation and keep the indoor temperature and humidity within predefined limits.

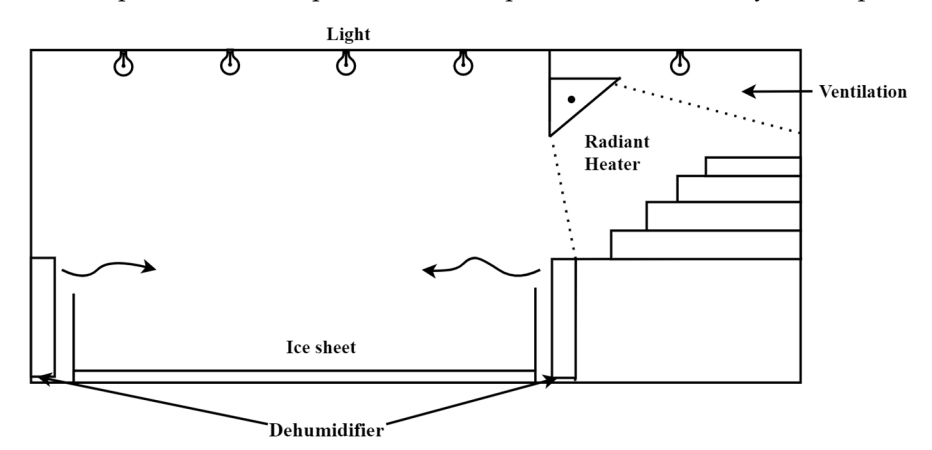


Figure 1. An indoor ice rink facility layout.

The model design comprehensively considers weather conditions, electricity price fluctuations, end-user preferences regarding equipment operation, and spectator schedules. With advancements in weather forecasting technologies and electricity market mechanisms, it is now feasible to obtain high-resolution weather predictions and real-time dynamic pricing data over short time horizons. These external inputs provide anticipatory guidance for system control [28].

Specifically, outdoor temperature, humidity and end-user preferences serve as boundary conditions for thermal and moisture load calculations, enabling the model to forecast future load variations and proactively adjust equipment scheduling. Time-varying electricity prices are incorporated into the objective function as dynamic cost coefficients, guiding equipment operation toward low-tariff periods to optimize electricity expenditure [29,30]. By integrating environmental signals with economic incentives, the proposed optimization model not only improves the precision of indoor thermal–humidity regulation but also enhances the overall operational efficiency and economic performance of the system. Figure 2 primarily illustrates the relationship between the proposed optimization model and the existing climate control system.

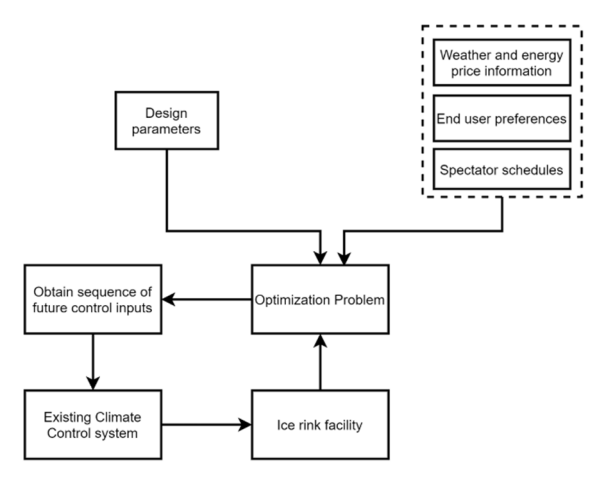


Figure 2. Overall architecture of the proposed optimization model and existing climate control system.

2.1. Objective Functions

Relevant studies have shown that reducing the energy consumption of building operational equipment can compromise daily comfort. Many studies aim to minimize cost

Algorithms 2025, 18, 446 6 of 28

or carbon emissions while maintaining user comfort. This study focuses on indoor ice rinks, aiming for both optimal comfort and cost efficiency, and explores climate control system strategies to find a balance between cost savings and improved comfort [31,32].

2.1.1. Users' Comfort in Spectator Stands Objective

The objective of the climate control system is to maintain the temperature and humidity of the spectator seating area within an acceptable deviation range. Relevant studies have shown that large fluctuations in indoor temperature and humidity can lead to thermal discomfort for occupants [33]. Based on this, the thermal comfort of users in the spectator seating area is expressed as follows:

$$F_1 = \min \sum_{t \in T} \left((\theta_z(t) - \theta_{z,set})^2 + (w_z(t) - w_{z,set})^2 \right)$$
 (1)

where $\theta_z(t)$ is the ambient temperature of the spectator stands at time t (K). Z area represents the spectator stands. $\theta_{z, set}$ is the set point temperature of the spectator stands (K). $w_z(t)$ is the humidity of spectator stands at time t (kg_{H2O}/kg_{air}). $w_{z,set}$ is the set point humidity of the spectator stands (kg_{H2O}/kg_{air}).

2.1.2. Economic Objective

The costs include operational costs and environmental costs. Operational costs cover electricity expenses, startup and shutdown-related costs, and maintenance costs.

$$F_2 = min(C_{ECO} + C_{sco}) \tag{2}$$

where C_{ECO} is operational cost and C_{sco} is environmental cost. The operational cost (C_{ECO}) is given as follows:

$$C_{ECO} = \sum_{t \in T} (\tau C_E(t) + \tau C_{OM}(t) + \tau C_{SC}(t))$$
(3)

where $C_E(t)$, $C_O(t)$, and $C_S(t)$ are cost of electricity consumption, maintenance, startup and shutdown of machine in time period t, respectively [34].

$$C_E(t) = C_E^{ven}(t) + C_E^{dh}(t) + C_E^{ht}(t)$$
 (4)

$$C_{OM}(t) = C_{OM}^{ven}(t) + C_{OM}^{dh}(t) + C_{OM}^{ht}(t)$$
 (5)

$$C_{SC}(t) = C_{SC}^{ven}(t) + C_{SC}^{dh}(t) + C_{SC}^{ht}(t)$$
(6)

where $C_E^{ven}(t)$, $C_E^{dh}(t)$, and $C_E^{ht}(t)$ are electricity costs of ventilation system, dehumidification, and radiant heating, respectively. $C_{OM}^{ven}(t)$, $C_{OM}^{dh}(t)$, and $C_{OM}^{ht}(t)$ are maintenance costs of ventilation system, dehumidification, and radiant heating, respectively. $C_{SC}^{ven}(t)$, $C_{SC}^{dh}(t)$, and $C_{SC}^{ht}(t)$ are startup and shutdown costs of the ventilation system, dehumidification, and radiant heating, respectively.

The ventilation system supplies air at a specified temperature and has a cooling unit. When the outdoor temperature exceeds the setpoint of the ventilation system, the cooling function is activated. When the outdoor temperature is below the setpoint, cooling is not applied.

$$C_E^{ven}(t) = \begin{cases} \frac{Q_{ven}}{COP} \times C_{ele}(t), \ \theta_{ex}(t) \ge \theta_z^{ven} \\ C_{ele}(t) \times P_{ven} \times S_{ven}(t), \ \theta_{ex}(t) < \theta_z^{ven} \end{cases}$$
(7)

$$C_E^{dh}(t) = C_{ele}(t) \times P_{dh} \times S_{dh}(t)$$
(8)

$$C_E^{ht}(t) = C_{ele}(t) \times P_{ht} \times S_{ht}(t)$$
(9)

Algorithms 2025, 18, 446 7 of 28

where Q_{ven} is the cooling load provided by the ventilation system. COP is the coefficient of performance of the ventilation system. $C_{ele}(t)$ is the electricity price at time t. P_{ven} , P_{dh} , and P_{ht} are the power of the ventilation system, dehumidifier, and radiation heaters, respectively (kW). $S_{ven}(t)$, $S_{dh}(t)$, and $S_{ht}(t)$ are binary variables for controlling the on/off state of the ventilation with a cooling unit, dehumidifier, and radiation heaters, respectively.

$$C_{OM}^{ven}(t) = C_{om-ven}(t) \times C_E^{ven}(t)$$
(10)

$$C_{OM}^{dh}(t) = C_{om-dh}(t) \times C_E^{dh}(t) \tag{11}$$

$$C_{OM}^{ht}(t) = C_{om-ht}(t) \times C_E^{ht}(t)$$
(12)

where $C_{om-ven}(t)$, $C_{om-dh}(t)$, and $C_{om-ht}(t)$ are cost coefficients of maintenance of ventilation, dehumidifier, and radiation heaters, respectively (CNY·kWh⁻¹).

$$C_{SC}^{ven}(t) = C_{sc-ven}(t) \times C_E^{ven}(t)$$
(13)

$$C_{SC}^{dh}(t) = C_{sc-dh}(t) \times C_E^{dh}(t)$$
(14)

$$C_{SC}^{ht}(t) = C_{sc-ht}(t) \times C_E^{ht}(t)$$
(15)

where $C_{sc-ven}(t)$, $C_{sc-dh}(t)$, and $C_{sc-dh}(t)$ are cost coefficients of startup and shutdown of ventilation, dehumidifier, and radiation heaters, respectively (CNY·kWh⁻¹). $\forall t \in T$. τ is a time interval (this study took 1 h (h)).

Environmental costs are driven by energy consumption, which, in the context of ice sports venues, primarily results from electricity usage. The most important emissions considered in the power generation industry, due to their effects on the environment, are SO₂, CO₂, and NO_x, which are modeled technically by the polynomial functions for the SO₂ emission, an emitted pollution model in tons per MW for CO₂, and an exponential function for NO_x emissions [35,36]. For the economic investigation of the adverse effects of electric power systems activities on climate change, various mechanisms, including penalties through carbon taxes or cap-and-trade systems, are used to mitigate gaseous pollutant emissions. The carbon tax mechanisms are imposed in some European countries, including Sweden (CAD 127/t) and Finland [37]. The taxes have been proposed in Canada at the provincial level, in Quebec and British Columbia (CAD 15/ton (in 2009) to CAD 30/ton (in 2012), respectively) [38]. This study represents the cost of the environment by constructing a CO₂ model. The carbon allowance price in the Chinese carbon market is stabilized at CNY 58/t CO₂. C_{sco} is given as follows:

$$C_{sco} = \left(\sum_{t \in T} (\tau C_E(t)) \cdot EF \cdot C_{co2}\right)$$
 (16)

where *EF* is the carbon emission factor for electricity (kg CO_2/kWh) and C_{co2} is the environmental cost of carbon emissions from electricity (CNY·kg CO_2^{-1}).

2.2. Constraint

2.2.1. Humidity Constraints

The humidity throughout the entire ice rink is maintained at a consistent level over a specified period of time. Since the humidity setpoint is measured based on relative humidity, and the environmental humidity of ice sports venues is designed using the parameter of relative humidity, while the measurement and adjustment of dehumidification equipment are based on specific humidity, it is necessary to convert between specific Algorithms 2025, 18, 446 8 of 28

humidity and relative humidity [39]. Constraints of indoor specific humidity are given as follows:

 $w_z(t) \le \phi_z^{max} \frac{0.622 * e z_{s(t)}}{P_{atm} - \phi_z^{max} * e z_{s(t)}}$ (17)

where $w_z(t)$ is humidity at time t in the studied area (kg_{H2O}/kg_{air}). \varnothing_z^{max} is the maximum relative humidity setpoint in the studied area (%). P_{atm} is atmospheric pressure (Pa). $ez_{s(t)}$ is the intermediate coefficient of conversion of temperature, relative humidity, and specific humidity. $ez_{s(t)}$ is given as follows:

$$ez_{s(t)} = 6.112 * e^{\frac{17.67*(\theta_z(t) - 273.15)}{\theta_z(t)}}$$
 (18)

where $\theta_z(t)$ is the temperature at time t in the studied area (K).

2.2.2. Temperature Constraints

The temperature in the spectator stands of ice sports venues must be maintained within the specified range. Constraints of temperature in the spectator stands are given as follows:

$$\theta_z^l \le Q_z(t) \le \theta_z^u \tag{19}$$

where θ_z^l and θ_z^u are the lower and upper limits of the temperature in the studied area, respectively (K).

2.2.3. Equipment Operating Constraints

To ensure indoor air quality and meet the practical operational needs of equipment in ice sports venues, this study incorporates a constraint into the optimization scheduling model requiring the ventilation system to be activated at least once per day. The ventilation system effectively replaces polluted indoor air accumulated from human activity and equipment operation, reducing the concentration of carbon dioxide, volatile organic compounds, and other harmful substances. This helps maintain a healthy indoor environment and safeguards the health and safety of both athletes and spectators.

$$S_{ven}(t) \ge 1 \tag{20}$$

2.3. Thermal Model

Due to the complex variations in temperature and humidity inside ice sports venues, an approximate physical model is constructed for indoor humidity and temperature in spectator stands of ice sports venues [9]. Due to the significant temperature difference between the spectator area and the space above the ice surface, the spectator area is treated as an independent thermal zone for study. The temperature in the spectator area varies considerably with seasonal changes, ranging from 8 °C to 26 °C, while the temperature above the ice surface remains around 16 °C at heights of 0.2 to 1.5 m and approximately 25 °C above 1.5 m. Given the need to maintain the spectator area's temperature under varying external conditions, it is reasonable to study it as an independent zone.

Based on the aforementioned building layout, dehumidification is not implemented in a zoned manner. Therefore, the spectator area shares the same humidity level as other zones.

2.3.1. Humidity Variation Model

(1) Calculation of Spectator Stands Humidity

Air humidity is influenced by the ventilation system through indoor and outdoor air exchange, air infiltration, and audience respiration. Additionally, the operation of

Algorithms 2025, 18, 446 9 of 28

dehumidifiers can remove part of the humidity. The specific humidity variation model is given as follows:

$$w_z(t) = w_z(t-1) + w_{ven}(t) + w_{leak}(t) + w_{aud}(t) - w_{dh}(t)$$
(21)

where $w_z(t-1)$ is air humidity in the ice sports venue at time t-1 (kg_{H2O}/kg_{air}). $w_{ven}(t)$ is the impact of the ventilation system on the humidity of the spectator stands (kg_{H2O}/kg_{air}). $w_{leak}(t)$ is the effect of air infiltration on the humidity of the spectator stands (kg_{H2O}/kg_{air}). $w_{aud}(t)$ is the moisture generated by audience respiration (kg_{H2O}/kg_{air}). $w_{dh}(t)$ is the effect of dehumidifier operation on the humidity of the spectator stands (kg_{H2O}/kg_{air}). The impact of the ventilation system on humidity is calculated as follows:

$$w_{ven}(t) = S_{ven}(t)\tau \frac{\dot{V} \times (w_{ex}(t) - w_{z}(t-1))}{V_{z}}$$
 (22)

where \dot{V} is the airflow rate of the ventilation system (m³/h). $w_{ex}(t)$ is the humidity of the incoming air, assuming the humidity of the air entering the ventilation system is the same as that of the outside air (kg_{H2O}/kg_{air}). V_z is the volume of air in the studied area (m³). $w_{ex}(t)$ is given as follows:

$$w_{ex}(t) = \frac{\emptyset_{ex}(t) * 0.622 * ex_{s(t)}}{P_{atm} - \emptyset_{ex}(t) * ex_{s(t)}}$$
(23)

where $\emptyset_{ex}(t)$ is the relative humidity of the outside air at time t (%). $ex_{s(t)}$ is the intermediate coefficient of conversion of temperature, relative humidity, and specific humidity outside. $ex_{s(t)}$ is given as follows:

$$ex_{s(t)} = 6.112 * e^{\frac{17.67*(\theta_{ex}(t) - 273.15)}{\theta_{ex}(t)}}$$
 (24)

where $\theta_{ex}(t)$ is the temperature of the outside air at time t (K). The effect of air infiltration on the humidity is given as follows:

$$w_{leak}(t) = \tau \frac{V_z^{leak} \times (w_{ex}(t) - w_z(t-1))}{V_z}$$
(25)

where V_z^{leak} is air leakage (m³/h). $w_{aud}(t)$ is given as follows:

$$w_{aud}(t) = \frac{N_s(t) \times N\varphi g \times \tau}{V_z \rho}$$
 (26)

where $N_s(t)$ is the occupancy rate of the venue (%). N is the total capacity of the ice sports venue (persons). φ is the clustering coefficient. g is the hourly moisture emission per person (kg/h). ρ is the air density (kg_{air}/m³). $w_{dh}(t)$ is given as follows:

$$w_{dh}(t) = \frac{v_z(t)S_{dh}(t)\tau}{V_z\rho} \tag{27}$$

where $v_Z(t)$ is the impact of dehumidifier operation on the moisture content of the air in the studied area (kg/h). $w_{ice}(t)$ is given as follows:

2.3.2. Temperature Variation Model

The temperature distribution inside ice sports venues is a complex phenomenon. To simulate the temperature changes in the spectator stands, many factors are considered, such as the ventilation system, the operation of radiant heating systems, heat loss through walls, air leakage, lighting, audience-generated heat, and the impact of heat loads such as

Algorithms 2025, 18, 446 10 of 28

radiative heat transfer between different areas [40,41]. The temperature variation model is given as follows:

$$\theta_z(t) = \theta_z(t-1) + \theta_{ht}(t) + \theta_{en}(t) + \theta_{ven}(t) + \theta_{light}(t) + \theta_{aud}(t) + \theta_{ref}(t)$$
 (28)

where $\theta_z(t)$ is the ambient temperature at time t (K). $\theta_z(t-1)$ is the ambient temperature at time t-1 (K). $\theta_{ht}(t)$ is the effect of radiant heating on temperature during an interval (K). $\theta_{en}(t)$ is the effect of outdoor air heat conduction through the envelope on temperature during an interval (K). $\theta_{ven}(t)$ is the effect of cooling air conditioning operation on temperature during an interval (K). $\theta_{light}(t)$ is the effect of lighting on temperature during an interval (K). $\theta_{aud}(t)$ is the effect of body heat dissipation on temperature during an interval (K). $\theta_{ref}(t)$ is the effect of ice temperature through thermal radiation on temperature (K). $\theta_{ht}(t)$ is given as follows:

$$\theta_{ht}(t) = \frac{P_{dh}S_{ht}(t)\tau \times 3.6}{m_z \times C_Z}$$
 (29)

where m_z is the mass of the air in the spectator stands (kg). C_Z is the specific heat capacity of air (commonly taken as 1.005 kJ/(kg·K)). m_z is given as follows:

$$m_z = V \times \rho \tag{30}$$

where *V* is the space volume (m³). ρ is the air density (kg/m³). $\theta_{en}(t)$ is given as follows:

$$\theta_{en}(t) = \frac{\left(UA + \dot{m}C_Z\right)(\theta_{ex}(t) - \theta_z(t-1))\tau}{m_z \times C_Z} \tag{31}$$

where U is the heat transfer coefficient of the building envelope (kW/(m²·K)). A is the surface area of the building envelope (m²). \dot{m} is the air leakage flow rate (m³/h). $\theta_{ex}(t)$ is the outdoor air temperature at time t (K). $\theta_{ven}(t)$ is given as follows:

$$\theta_{ven}(t) = \frac{Q_{ven} \times \tau}{m_z \times C_Z} \tag{32}$$

where Q_{ven} is the heat transferred by the ventilation system (K). Q_{ven} is given as follows:

$$Q_{ven} = \dot{v} \times C_Z \times S_{ven}(t)(\theta_z^{ven} - \theta_z(t-1))$$
(33)

where θ_z^{ven} is the setpoint temperature for ventilation system (K). \dot{v} is the air mass flow rate (kg/h). $\theta_{light}(t)$ is given as follows:

$$\theta_{light}(t) = \frac{P_{light} \times \tau}{m_z \times C_Z} \tag{34}$$

where P_{light} is the total power of the light in the spectator stands (kW). $\theta_{aud}(t)$ is given as follows:

$$\theta_{aud}(t) = \frac{q_{rad} \times N_{aud}(t) \times N_{max}}{m_z \times C_Z}$$
(35)

where q_{rad} is the heat generated by indoor occupants (W/(h·Person)). $N_{aud}(t)$ is the schedule of audience occupancy as a percentage (%). N_{max} is the maximum capacity of the audience (Person).

According to the Stefan–Boltzmann thermodynamic law, the total energy radiated per unit area from the surface of a black body per unit time is proportional to the fourth power of the black body's thermodynamic temperature T. Thermal radiation originating from the near-ice area, ceiling, and spectator stands contributes to the temperature rise in the

Algorithms 2025, 18, 446 11 of 28

spectator stands. To better calculate the thermal radiation between these areas, the near-ice area is designated as zone X, the ceiling area as zone Y, and the spectator stands as zone Z. The influence of the thermal radiation from the ice temperature on the temperature of the spectator stands (zone Z) is calculated using shape factors (F) and surface radiation quantities (Q). $\theta_{ref}(t)$ is given as follows:

$$\theta_{ref}(t) = \frac{(A_{x,z}F_{x,z}(Q_x - Q_z) + A_{y,z}F_{y,z}(Q_y - Q_z)) \times \tau}{m_z \times C_Z}$$
(36)

where Q_x , Q_y , and Q_z are the radiative heat of the surfaces in zones X, Y, and Z, respectively. $A_{x,z}$ is the contact area between zones X and Z (m²). $A_{y,z}$ is the contact area between zones Y and Z (m²). $F_{x,z}$ is the shape factor between zones X and Z. $F_{y,z}$ is the shape factor between zones Y and Z. Q_x is given as follows:

$$Q_x = \epsilon \sigma \theta_x^4(t) \tag{37}$$

where ϵ is the emissivity coefficient. σ is the proportional constant (kW/m²). $\theta_x(t)$ is the temperature of zone X at time t (K). $F_{x,z}$ is given as follows:

$$F_{x,z} = \frac{1}{W_{x,z}\pi} \begin{pmatrix} W_{x,z}tan^{-1} \frac{1}{W_{x,z}\pi} + H_{x,z}tan^{-1} \frac{1}{H_{x,z}\pi} - \sqrt{H_{x,z}^{2} + W_{x,z}^{2}}tan^{-1} \sqrt{\frac{1}{H_{x,z}^{2} + W_{x,z}^{2}}} \\ + \frac{1}{4} \begin{pmatrix} \frac{(1+W_{x,z}^{2})(1+H_{x,z}^{2})}{1+H_{x,z}^{2} + W_{x,z}^{2}} \left[\frac{W_{x,z}^{2}(1+H_{x,z}^{2} + W_{x,z}^{2})}{(1+W_{x,z}^{2})(W_{x,z}^{2} + H_{x,z}^{2})} \right]^{W_{x,z}^{2}} \\ \cdot \left[\frac{H_{x,z}^{2}(1+H_{x,z}^{2} + W_{x,z}^{2})}{(1+H_{x,z}^{2})(W_{x,z}^{2} + H_{x,z}^{2})} \right]^{H_{x,z}^{2}} \end{pmatrix}$$
(38)

where $W_{x,z}$ is given as follows:

$$W_{x,z} = \frac{w_{x,z}}{l_{x,z}} \tag{39}$$

and $H_{x,z}$ is given as follows:

$$H_{x,z} = \frac{h_{x,z}}{l_{x,z}} \tag{40}$$

where $w_{x,z}$ is the width of the vertical plane of the contact surface between zones X and Z. $l_{x,z}$ and $h_{x,z}$ are the width and height of the contact surface of zone Z, respectively. The schematic diagram is presented in Figure 3.

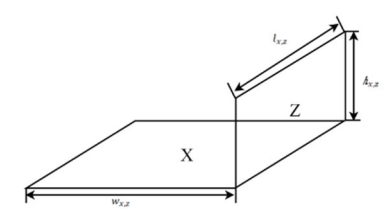


Figure 3. Geometric configuration diagram.

 $F_{y,z}$, $W_{y,z}$, $H_{y,z}$, $w_{y,z}$, $l_{y,z}$, and $h_{y,z}$ are the same as those for the relationship between zone Y and zone Z.

2.4. Solution Algorithm

The calculation and optimization processes are conducted on the Python 3.10 platform, which is shown in Figure 4.

2.4.1. Solution Procedure for Multi-Objective Optimization

In this work, three algorithms, NSGA-II, standard MOEA/D, and Brown Bear Optimization, are selected to solve the Climate Control Systems Scheduling for Indoor Ice Sports Venues' Spectator Zones problem.

• NSGA-II algorithm

The NSGA-II (Non-dominated Sorting Genetic Algorithm II), a widely used intelligent optimization algorithm, is adopted to solve the Pareto frontier of the proposed model [42–45]. The NSGA-II algorithm effectively identifies the optimal solution set, with its core mechanism based on the selection and population update processes guided by each individual's non-dominated rank and crowding distance within the population. The NSGA-II algorithm is characterized by its high efficiency and the use of an elitism strategy to ensure the quality of solutions.

The main decision factors for selecting specific parameter values in the NSGA-II operation include population size, selection process, crossover probability, mutation probability, and the number of iterations.

Step 1: Initialization. Generate initial populations. Each individual in the population is a feasible operating scheme. The content of the scheme is the start and stop state of the equipment on a time-by-time basis. Code each individual. Calculate the objective function for each individual.

Step 2: Fast Undominated Sorting. Sort all individuals as non-dominated and then divide them into a number of Pareto ranks. Select the high rank as the current optimal solution set. Calculate the crowding distance for each individual, which is used to maintain population diversity.

Step 3: Select. The binary tournament selection (BTS) process is based on two key factors: rank and crowding distance. The subsequent selection of parental individuals is made for the purpose of crossover and mutation operations.

Step 4: Crossover and variation. The utilization of simulated binary crossover (SBX) with polynomial variation facilitates the generation of a population of offspring. It is imperative that all newly generated individuals satisfy the imposed constraints.

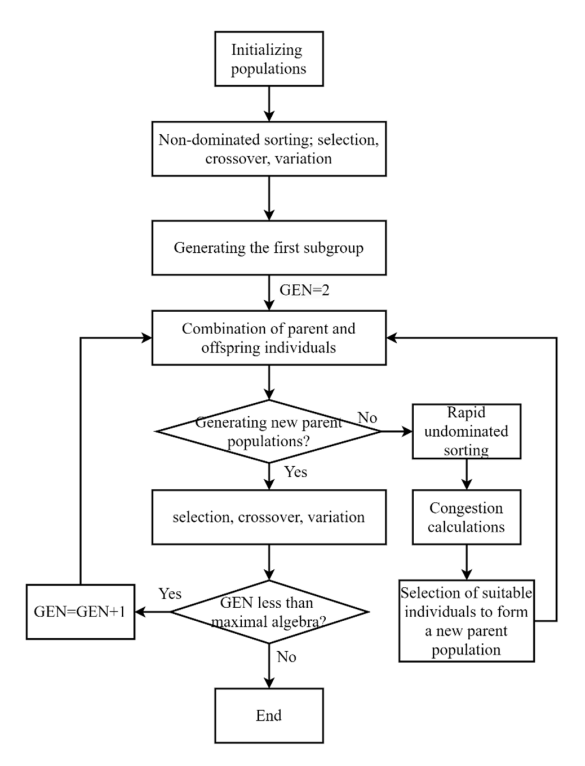


Figure 4. Flowchart of the Non-dominated Sort Genetic Algorithm with elitist strategy (NSGA-II).

Step 5: Elite retention and population renewal. The subsequent step in the process is the amalgamation of the parent and child populations. Subsequent to this, non-dominated sorting should be performed on the newly formed population. It is recommended that individuals with high Pareto rank and high crowding are retained in order to ensure convergence and diversity.

Stage 6: Termination of the proceedings. Upon attaining the maximum permitted number of iterations, the process is terminated. The final output is the set of non-dominated solutions, i.e., the Pareto front of the optimal scheme solution. Specifically, (1) the population size should not be set too large or too small. When it is set too small, it is difficult to find the actual shortest path; when it is set too large, the computation time is longer and the convergence tendency is accelerated, but it is easy to fall into the local optimal solution. (2) The crossover probability determines the average number of individuals involved in mating during the evolutionary process. If it is set too high, the algorithm becomes overly random and may lose its search direction. If it is set too low, the convergence speed becomes too slow. (3) The smaller the mutation probability is, the slower the convergence speed becomes. The larger the mutation probability, the more genetic variation occurs. Mutation has a destructive effect on the optimal solution. If the mutation probability is too large, it may cause better search conditions to degrade into worse ones. (4) If the number of iterations is too small, it is difficult to converge to the optimal solution. Increasing the number of iterations can speed up the convergence, but if the number of iterations is too high, it will be difficult to obtain the global optimal solution.

• Multi-Objective evolutionary algorithm based on Decomposition (MOEA/D)

The Multi-Objective evolutionary algorithm based on Decomposition (MOEA/D) uses an aggregation function to generate a set of uniform weight vectors, through which the multi-objective optimization problem is divided into a set of single-objective sub-problems, and then updates the "bad solutions" in the neighborhood according to the value of the aggregation function so as to ultimately find the optimal Pareto solution set [23]. The steps are as follows:

Step 1: Initialization. Initialize the population and calculate the objective function value. Generate a set of weight vectors and define neighborhoods (e.g., based on weight distances or solution spaces) for each subproblem. Determine the ideal point (minimum set of objective values).

Step 2: Subproblem co-optimization. For each subproblem (corresponding to a weight vector), randomly select two solutions from the neighborhood and use DE or SBX+ variant to generate child solutions. Evaluate and update the optimal solutions and ideal points in the neighborhood according to aggregation functions (e.g., Tchebycheff, weighted sum) as needed.

Step 3: Population update. Update the solutions in the neighborhood of all subproblems after each generation.

Step 4: Judgment termination. Repeat steps 2–3 until the maximum number of generations or function evaluations is satisfied.

• Multi-Objective Brown Bear Optimization (MOBBO)

MOBBO is a novel multi-objective optimization algorithm based on the foraging, territory marking, and sniffing behavior of brown bears. The algorithm simulates the natural strategy of "exploration-exploitation" balance in the foraging process of brown bears and has the ability of both global search and local exploitation. In order to effectively deal with the multi-objective optimization problem, MOBBO introduces the non-dominated sorting and external archive strategies to dynamically maintain the optimal non-dominated solution set and improve the diversity and balance of the solution set. With the help of the ε -domination mechanism, the algorithm can effectively prevent the aggregation of

Algorithms 2025, 18, 446 14 of 28

solutions while ensuring the quality of the solution set, which is suitable for problems with complex constraints and multi-objective engineering optimization.

Step 1: Initialization. Randomly generate the population and initialize the tread markers, i.e., decision variables. Set the objective function, population size, range of design variables, and termination criteria.

Step 2: Non-dominated sorting and profile initialization. Perform Pareto sorting to identify non-dominated solutions and initialize the external archive. Filter the set of solutions through the ε -domination mechanism to ensure that the solutions retained in the external archive are distributed equally in the target space.

Step 3: Iterative evolution. In each iterative generation, sequentially perform treadmarking behavior (alternating exploration and exploitation), sniffing behavior (local fine search), and updating the nondominated ordering and external archive. After each step, the better solution is retained by greedy selection.

(1) Footprint Scent Marking Behavior

Characteristic Gait Walking (First One-Third of Iterations)

$$P_{i,j,k}^{new} = P_{i,j,k}^{old} - \left(\theta_k \cdot \alpha_{i,j,k} \cdot P_{i,j,k}^{old}\right) \tag{41}$$

$$\theta_k = \frac{C_t}{N_t} \tag{42}$$

where $\alpha_{i,j,k}$ is a random number within the range; C_t is the current iteration number; and N_t is total number of iterations.

Cautious Stepping Feature (From One-Third to Two-Thirds of Iterations)

$$P_{i,j,k}^{new} = P_{i,j,k}^{old} + F_k \cdot \left(P_{j,k}^{best} - L_k \cdot P_{j,k}^{worst} \right) \tag{43}$$

$$F_k = \beta_{1,k} \cdot \theta_k \tag{44}$$

$$L_k = \text{round}(1 + \beta_{2,k}) \tag{45}$$

where $\beta_{1,k}$ and $\beta_{2,k}$ are random numbers within the range [0, 1]; F_k is the step factor at the k-th iteration; and L_k is the step size at the k-th iteration.

Twisting Footsteps Feature (Final One-Third of Iterations)

$$P_{i,j,k}^{new} = P_{i,j,k}^{old} + \omega_{i,k} \cdot \left(P_{j,k}^{best} - \left| P_{i,j,k}^{old} \right| \right) - \omega_{i,k} \cdot \left(P_{j,k}^{worst} - \left| P_{i,j,k}^{old} \right| \right)$$

$$\tag{46}$$

$$\omega_{i,k} = 2\pi\theta_k \gamma_{i,k} \tag{47}$$

where $\gamma_{i,k}$ is a random number within the range [0, 1], and $\omega_{i,k}$ is the twisting angular velocity of the *i*-th individual at iteration *k*.

(2) Sniffing Behavior

The mathematical model of brown bear sniffing behavior is as follows:

$$P_{m,j,k}^{new} = \begin{cases} P_{m,j,k}^{old} + \lambda_{j,k} \cdot \left(P_{m,j,k}^{old} - P_{n,j,k}^{old}\right), f\left(P_{m,k}^{old}\right) < f\left(P_{n,k}^{old}\right) \\ P_{m,j,k}^{new} = P_{m,j,k}^{old} + \lambda_{j,k} \cdot \left(P_{n,j,k}^{old} - P_{m,j,k}^{old}\right), f\left(P_{m,k}^{old}\right) \ge f\left(P_{n,k}^{old}\right) \end{cases}$$

$$(48)$$

where $\lambda_{j,k}$ is a random number within the range [0, 1].

Step 4: Termination and Output. Terminate when the maximum number of iterations is reached or there is no improvement, and output the optimal Pareto solution set.

To comprehensively evaluate the performance of the multi-objective optimization algorithms used in this study, three widely recognized performance metrics were selected:

computational time, Hypervolume (HV), and Inverted Generational Distance (IGD) [46,47]. These metrics, respectively, assess the computational efficiency, the diversity and convergence of the obtained solution sets, and the proximity of the solutions to the true Pareto front.

The Hypervolume (HV) metric measures the volume of the objective space covered by the obtained solutions and reflects both convergence and diversity. Its formula is defined as follows:

$$HV = \text{Lebesgue measure}\left(\bigcup_{x \in P} [f_1(x), r_1] \times [f_2(x), r_2] \times \ldots \times [f_m(x), r_m]\right)$$
(49)

where P is the current set of non-dominated solutions (Pareto front); $f_i(x)$ is the value of solution x in the i-th objective; $r = (r_1, r_2, \ldots, r_m)$ is the reference point, usually chosen as a worst-case point in the objective space; and m is the number of objectives. A larger HV value indicates a better-performing solution set.

The Inverted Generational Distance (IGD) metric evaluates the proximity and diversity of the obtained solutions with respect to the true Pareto front. Its formula is given by:

$$IGD(P, P^*) = \frac{1}{|P^*|} \sum_{v \in P^*} \min_{u \in P} d(u, v)$$
 (50)

where P is the obtained non-dominated solution set; P^* is the true or reference Pareto-optimal solution set; d(u,v) denotes the Euclidean distance between solutions u and v; and $|P^*|$ is the number of solutions in the reference set. A smaller IGD value indicates better convergence and distribution of the solution set.

2.4.2. A TOPSIS-Based Method for Optimal Selection

The TOPSIS method, also known as the approximate ideal solution ranking method, is a typical Multi-Criteria Decision-Making (MCDM) approach [48–50]. By applying the multi-objective optimization algorithm, the Pareto solution set of the problem can be obtained, and then TOPSIS is used to filter out the optimal solution. The multi-objective optimization algorithm fully explores the solution space to ensure the diversity and global nature of the solution set, while TOPSIS introduces a clear sorting logic in the solution set to make the screening process of optimal solutions clearer and more efficient, which not only avoids the nuisance of manual subjective selection but also improves the decision-making utility of the solution. The steps are as follows:

Step 1: The total number of alternative schemes is n. Moreover, there are m elements in the scheme. The alternative schemes are represented in matrix format. x_{ij} denotes the attribute of the i-th scheme under the criterion C_i , with incomparable units.

$$A_{i} = \begin{pmatrix} x_{11}, \dots & x_{1j}, \dots & x_{1m} \\ x_{i1}, \dots & x_{ij}, \dots & x_{im} \\ x_{n1}, \dots & x_{ni}, \dots & x_{nm} \end{pmatrix} i = 1, 2, \dots, n; j = 1, 2, \dots, m$$
 (51)

Step 2: Normalize x_{ij} to ensure consistency. The normalization rules are as follows: For benefit criteria (the larger the value, the better):

$$u_{ij} = \frac{x_{ij} - \min\{x_{ij}\}}{\max\{x_{ij}\} - \min\{x_{ij}\}}$$
 (52)

Algorithms 2025, 18, 446 16 of 28

where u_{ij} is the normalized value of x_{ij} ; $max\{x_{ij}\}$ is the maximum value of x_{ij} across all alternatives for the criterion C_j ; and $min\{x_{ij}\}$ is the minimum value of x_{ij} across all alternatives for the criterion C_j .

For cost criteria (the smaller the value, the better) the following expression is derived:

$$u_{ij} = \frac{\max\{x_{ij}\} - x_{ij}}{\max\{x_{ij}\} - \min\{x_{ij}\}}$$
 (53)

Step 3: Normalize the matrix by processing each element as a vector. The normalization is performed as follows:

$$r_{ij} = \frac{u_{ij}}{\sqrt{\sum_{i=1}^{n} u_{ij}^2}} \tag{54}$$

Step 4: To calculate the weighted normalized decision matrix, apply the weights w_j to each element of the normalized matrix. The elements of the weighted normalized decision matrix are calculated as follows:

$$z_{ij} = w_j u_{ij} \tag{55}$$

Step 5: Identify the ideal solution and anti-ideal solution as follows:

$$A^{+} = \left\{ z_{1}^{+}, z_{2}^{+}, \dots, z_{j}^{+}, \dots, z_{m}^{+} \right\} = \left\{ \max z_{i1}, \max z_{i2}, \dots, \max z_{im} \right\}$$
 (56)

$$A^{-} = \left\{ z_{1}^{-}, z_{2}^{-}, \dots, z_{j}^{-}, \dots, z_{m}^{-} \right\} = \left\{ \min z_{i1}, \min z_{i2}, \dots, \min z_{im} \right\}$$
 (57)

Step 6: Calculate Euclidean distances between each alternative and ideal and antiideal solution.

$$D_i^+ = \sqrt{\sum_{j=1}^n \left(z_{ij} - z_j^+\right)^2}$$
 (58)

$$D_i^- = \sqrt{\sum_{j=1}^n \left(z_{ij} - z_j^-\right)^2} \tag{59}$$

Step 7: Calculate the distance to the ideal solution for each alternative.

$$D_i^+ = \frac{D_i^-}{D_i^+ + D_i^-} \tag{60}$$

The scheme with the largest ideal proximity value represents the optimal scheme, specifically referring to the optimal operational equipment scheme for the climate control system in ice sports venues.

3. Case Study

3.1. Case Description

To verify the effectiveness and applicability of the multi-objective optimization method, a simulation was conducted on an ice hockey arena in a cold region of China. The arena features an ice surface area of 1800 square meters, measuring 30 m in width and 60 m in length, and is equipped with 6 rows of bleachers. It serves as a training facility and includes 205 spectator seats. Parameters are given in Table 1.

Table 1. Parameter of the equipment and ice sports venue.

Parameter	Value	Unit	Parameter	Value	Unit
	288.15 (Winter);				
$ heta_{z,set}$	291.15 (Transition season) 293.15 (Summer)	K	U	0.00044	$kW/(m^2 \cdot K)$
$w_{z,set}$	0.0845	kg _{H2O} /kg _{air}	A	1937.49	m^2
P_{ven}	200	kW	m	193.452	kg/h
P_{dh}	70	kW	\dot{v}	1225	kg/h
P_{ht}	176	kW	q_{rad}	0.18	kW/(h·Person)
au	1	h	N_{aud}	205	Person
\varnothing_z^{max}	70 (Summer); 60 (Transition season, Winter)	%	ϵ	1	-
\dot{V}	60	kg/s	σ	0.00567	kW/m^2
V_z^{leak}	157.92	m ³ /h	$\theta_{x}(0)$	279.15	K
N	261	Person	$\theta_y(0)$	293.15	K
			9(-)	288.15 (Winter,	
φ	0.92	-	$ heta_z(0)$	Transition season); 293.15 (Summer)	K
8	0.391	kg/h	$w_z(0)$	0.0745	kg_{H2O}/kg_{air}
8	0.051	1.6/11	u 2(0)	293.15 (Summer)	1807 18air
ρ	1.225	kg/m ³	$ heta_z^{ven}$	283.15 (Winter) 285.15 (Transition	K
				season)	
$v_Z(t)$	120	kg/h	$C_{om-ven}(t)$	0.0045	$CNY\cdot kWh^{-1}$
K	0.828	kg/m ² ⋅h	$C_{om-dh}(t)$	0.0105	$CNY\cdot kWh^{-1}$
A_{ice}	1800	m^2	$C_{om-ht}(t)$	0.0037	CNY⋅kWh ⁻¹
X_a	0.0189	kg _{H2O} /kg _{air}	$C_{sc-ven}(t)$	0.0024	$CNY\cdot kWh^{-1}$
X_i	0.00245	kg _{H2O} /kg _{air}	$C_{sc-dh}(t)$	0.0058	$CNY\cdot kWh^{-1}$
T_{ice}	268.15	K	$C_{sc-dh}(t)$	0.0065	$CNY \cdot kWh^{-1}$
100	281.15 (Winter)		sc un ()		
$ heta_z^l$	283.15 (Transition season);	K	EF	0.5688	$CO_2 \cdot kWh^{-1}$
~	285.15 (Summer)				_
	291.15 (Winter),				
$ heta_z^u$	293.15 (Transition season);	K	C_{co2}	0.058	CNY·kg CO ₂
_	299.15 (Summer)				<u> </u>
C_Z	1.005	$kJ/(kg\cdot K)$	COP	3	

3.2. Data Source of Weather and Electricity Price

To simulate the running state of equipment in ice sports venues based on outdoor climatic conditions, it is essential to select suitable hourly meteorological parameters. Given the stochastic nature of meteorological conditions, using weather data from a specific year to calculate the model may lead to results that lack representativeness. To ensure the results reflect long-term climatic characteristics, typical year meteorological data are chosen for the calculations [51]. Data were obtained from https://climate.onebuilding.org (accessed on 14 July 2025), where climate data are regularly updated, validated, and subjected to quality checks. The validation process is primarily based on the 2021 ASHRAE Handbook. This data source has been widely applied in numerous studies.

For this research, typical days of summer, winter, and transitional seasons in cold regions are selected for simulation. Apart from winter and summer, this study follows previous research by combining spring and autumn into a single transitional season for analysis. The outdoor ambient temperature and relative humidity of the three typical days are shown in Figure 5. During typical summer days, ambient conditions are characterized by high temperatures and elevated humidity levels. In contrast, transitional seasons exhibit moderate temperature and humidity conditions, while typical winter days are marked by both low temperatures and low humidity.

Algorithms 2025, 18, 446 18 of 28

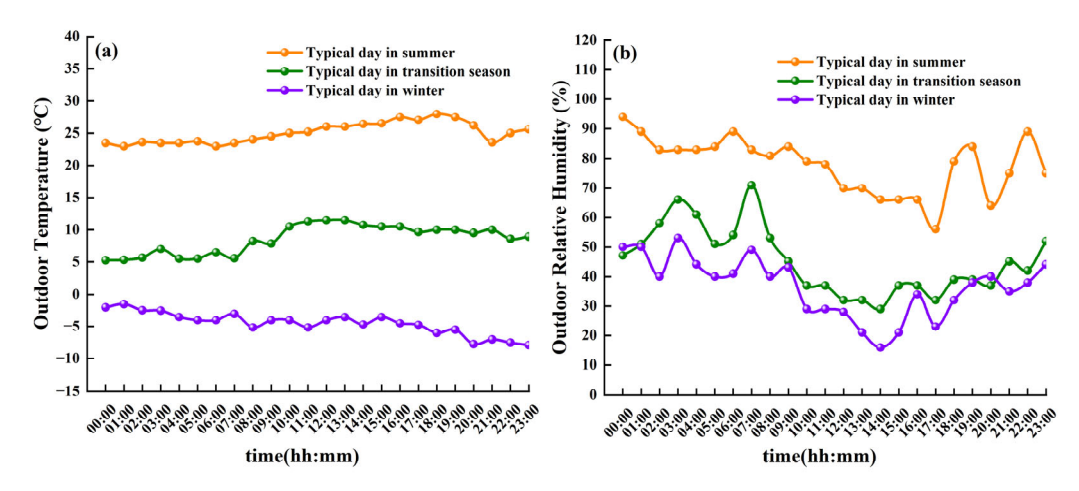


Figure 5. Outdoor temperature and relative humidity of typical days: (a) Outdoor temperature; (b) Outdoor relative humidity.

Based on the optimization models as shown in Equation (4), the technical input parameters are given in Table 2.

Table 2. Electricity tariffs of the grid.

Time Period	Time	Electricity Tariffs (CNY/kWh)
Peak	10:00–13:00, 17:00–22:00	1.71
Flat	7:00–10:00, 13:00–17:00, and 22:00–23:00	1.00
Valley	23:00–24:00, 0:00–7:00	0.36

3.3. Results

3.3.1. Pareto Frontiers

In order to comprehensively evaluate the performance of different multi-objective optimization algorithms, three commonly used evaluation metrics, namely, computation time, Hypervolume (HV), and Inverted Generational Distance (IGD), are selected for comparative analysis in this work. Among them, the computation time reflects the operation efficiency of the algorithm; HV measures the breadth and diversity of the distribution of the solution set, and the larger value represents the better quality of the solution set; and IGD measures the proximity between the solution set and the theoretical optimal solution, and the smaller value indicates the better convergence of the solution set.

The comparison results of the three multi-objective optimization algorithms NSGA-II, MOEA/D, and MOBBO in terms of computation time, Hypervolume (HV), and Inverted Generational Distance (IGD) are shown in Table 3. In terms of computation time, MOEA/D has the highest running efficiency of 86.21 s, which is better than NSGA-II (295.85 s) and MOBBO (237,860.78 s). However, in terms of solution set diversity and convergence, NSGA-II performs the most outstandingly, with an HV value of 6946.8083, which is significantly better than the other algorithms, showing excellent solution set expansion capability, while the lowest IGD value (10.4241) indicates its excellent convergence characteristics in terms of approaching the optimal frontier.

Table 3. Comparison of performance metrics (time, HV, IGD) among NSGA-II, MOEA/D, and MOBBO algorithms.

Metrics	NSGA-II	MOEA/D	MOBBO
Time	295.85 s	86.21 s	237,860.78 s
HV	6946.8083	506.7154	4567.56
IGD	10.4241	161.1774	62.13

Considering computational efficiency, solution set diversity, and convergence, NSGA-II is finally selected as the optimal solution algorithm in this work. Although its computation time is slightly higher than that of MOEA/D, NSGA-II has obvious advantages in the quality of the solution set and convergence, which are the core indexes of multi-objective optimization, and it is more suitable for the application of optimal scheduling of the ice rink climate control system in this study. In this study, the initial population size was set to 200 and the number of iterations to 1000. These parameters were carefully selected based on multiple rounds of testing and tuning. The results showed that this configuration strikes an appropriate balance between solution quality and computational efficiency. It ensures sufficient convergence of the optimization process while effectively controlling the computational time, thus avoiding both premature convergence and excessive computational cost.

Figure 6 shows the Pareto front obtained under typical temperature and humidity conditions by applying the NSGA-II algorithm [52].

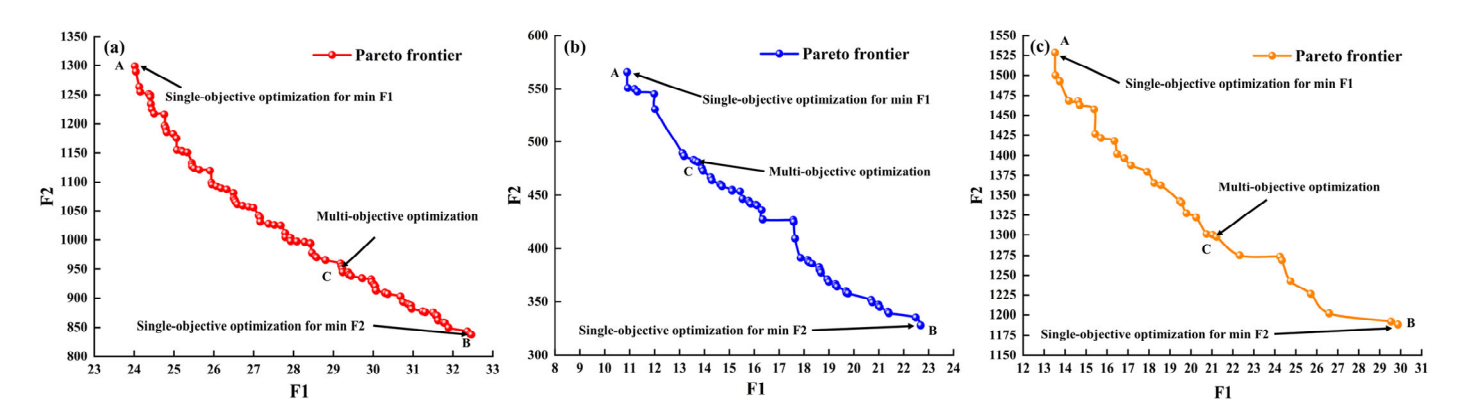


Figure 6. Pareto optimal chart of three typical days: (a) typical day in summer; (b) typical day in transitional season; and (c) typical day in winter.

Figure 6 illustrates the best Pareto fronts for multi-objective optimization of the operation of the ventilation, dehumidification, and radiant heating equipment for the spectator stand of an ice sports arena under typical days in summer, transitional seasons, and winter. On each Pareto frontier, the single-objective optimal solutions are specifically denoted as points A and B, while the multi-objective compromise solution is marked as point C. Among them, schemes A and B represent extreme scenarios: Scheme A achieves the highest level of thermal comfort at the expense of the highest cost, whereas Scheme B minimizes economic expenditure but yields relatively lower comfort. Across all three typical days, a clear trade-off relationship between comfort and cost is observed—enhancing indoor thermal comfort inevitably leads to increased equipment operation costs.

Table 4 presents the scheduling objectives under three optimization scenarios: maximum comfort, minimum cost, and the compromise solution selected using the TOPSIS method. As shown, on three typical days, when the indoor environment was optimized to the maximum comfort level, the operating cost exceeded the optimal cost value by at least 28.5%. On the contrary, when the operating costs were reduced to the minimum, the changes in temperature and humidity increased by at least 35.13% respectively compared to their respective optimal comfort levels, which was detrimental to the economic benefits of maintaining the system's operation. In contrast, the multi-objective optimization model achieves a balanced performance: although its economic cost and comfort are slightly inferior to those of the single-objective optimal solutions, it effectively harmonizes operational economy with indoor environmental comfort.

Objective	Maximum Comfort		Minimum Cost		TOPSIS	
Objective	F1	F2	F 1	F2	F1	F2
Typical day in summer	24.02	1298.7	32.46	837.86	29.21	954.56
Typical day in transition season	10.92	565.34	22.68	327.98	13.75	481.32
Typical day in winter	13.52	1528.33	29.87	1189.40	21.22	1297.45

Table 4. Economic cost and thermal comfort of different optimizations.

Compared with the model optimized solely for users' comfort, the multi-objective optimization model improves economic performance under typical summer, transitional, and winter conditions by 26.5%, 14.9%, and 15.1%, respectively. In contrast, compared with the cost-optimal model, it reduces spectators' discomfort under the same three typical conditions by 10.0%, 39.3%, and 28.9%, respectively. Therefore, the multi-objective optimization model demonstrates a superior ability to balance economic efficiency and users' comfort, outperforming single-objective models under varying climatic scenarios.

3.3.2. Optimal Scheduling Results Analysis

Figure 7 illustrates the power scheduling of the system under three scenarios: maximum comfort, minimum cost, and multi-objective optimization. Under extremely hot and humid weather conditions, in order to maintain user comfort, the ventilation system operates at nearly full power, while the radiant heating system remains largely inactive. The primary variation in climate control system load arises from the operation of the dehumidification and ventilation systems.

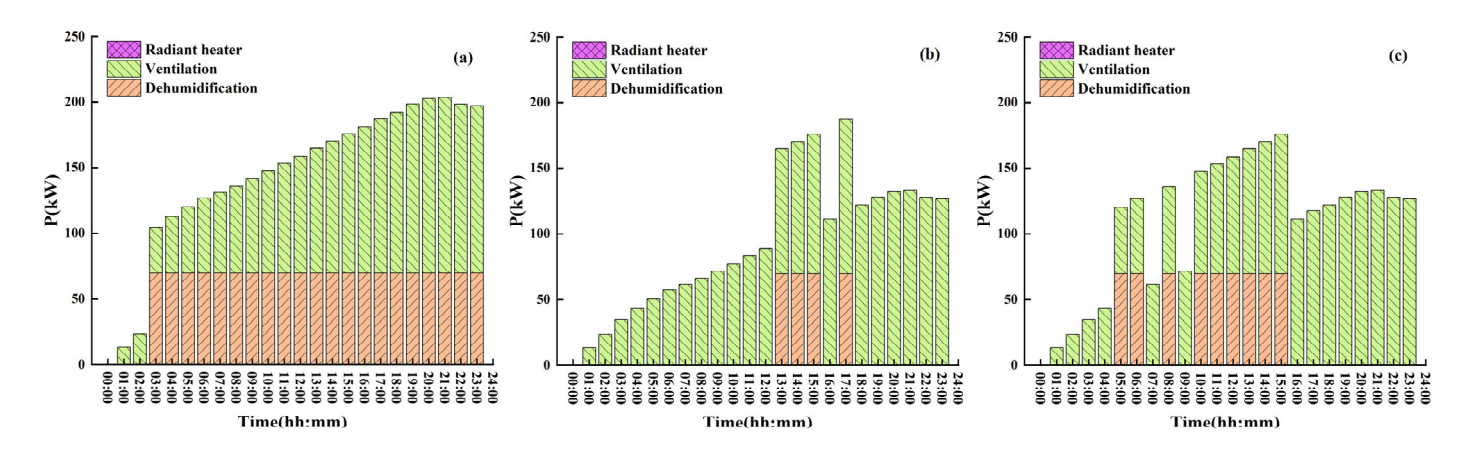


Figure 7. Optimized scheduling results of a typical day in summer: (a) single-objective optimization (F1); (b) single-objective optimization (F2); and (c) multi-objective optimization.

As shown in Figure 7a, user comfort is maintained at the highest level, with the dehumidification system operating continuously throughout the day. To ensure comfort, this scenario maintains high ventilation rates and strict humidity control at all times, reflecting a tightly constrained operational logic that leads to a significant increase in overall power demand and system operating costs.

In contrast, Figure 7b shows that the dehumidification system is activated only during 13:00–15:00 and 17:00–18:00. This scenario clearly prioritizes economic efficiency by reducing the duration of dehumidification, thereby lowering operating costs at the expense of user comfort.

Figure 7c presents the power scheduling under the multi-objective optimization scenario. Compared to Figure 7a, dehumidification operation is reduced during certain morning hours, resulting in a shorter total dehumidification duration. Compared to

Figure 7b, however, dehumidification is increased in several time periods, leading to a longer total operating time. This indicates that the multi-objective strategy effectively balances comfort and cost.

The scheduling results of a typical day in a transitional season are shown in Figure 8. Under moderate outdoor temperature and relative humidity conditions, ventilation and radiant heaters are activated to maintain user comfort, while the dehumidification system remains inactive.

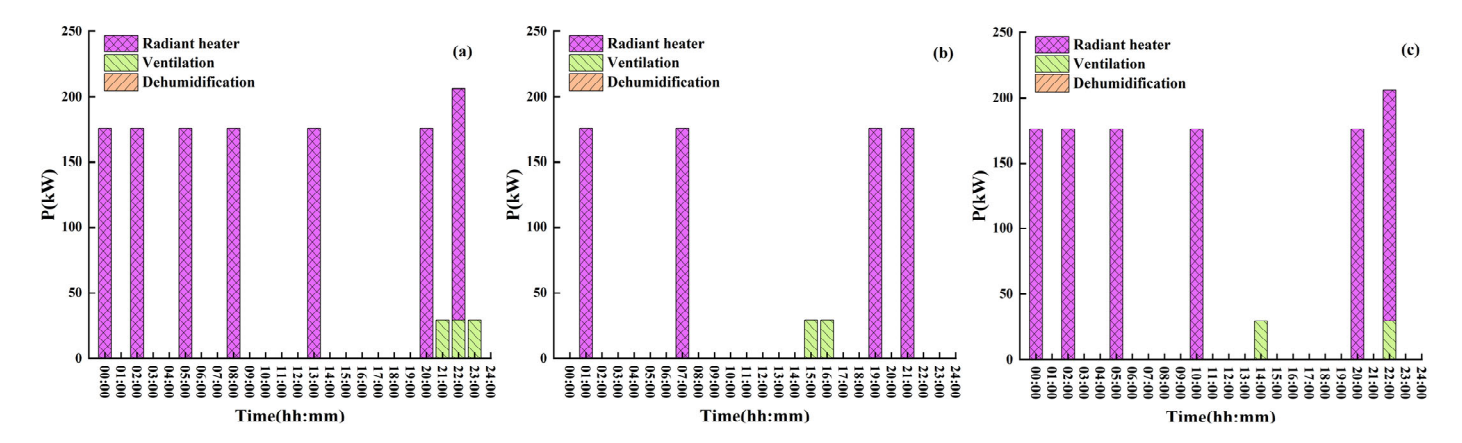


Figure 8. Optimized scheduling results of a typical day in a transitional season: (a) single-objective optimization (F1); (b) single-objective optimization (F2); and (c) multi-objective optimization.

As shown in Figure 8a, the radiant heaters operate during seven time intervals throughout the day (00:00–01:00, 02:00–03:00, 05:00–06:00, 08:00–09:00, 13:00–14:00, 20:00–21:00, and 22:00–23:00), while the ventilation system runs only in the evening from 21:00 to 24:00.

In contrast, Figure 8b shows radiant heating activated during four intervals (01:00–02:00, 07:00–08:00, 19:00–20:00, and 21:00–22:00), with ventilation limited to the afternoon period from 15:00 to 17:00. This scenario clearly prioritizes economic efficiency by reducing the operation time of both radiant heating and ventilation, thereby lowering costs at the expense of user comfort.

Figure 8c illustrates the power scheduling under the multi-objective optimization scenario. Compared to scenario A, both the durations of radiant heating and dehumidification operations are reduced. In contrast, compared to scenario B, the operation times for both radiant heating and dehumidification are increased, with dehumidification strategically scheduled during peak load periods.

The scheduling results of a typical day in winter are shown in Figure 9. As shown in Figure 9a, the radiant heating system operates frequently throughout the day with frequent start–stop cycles to maintain user comfort, serving as the primary source of electrical load. The dehumidification system is activated only at 00:00–1:00, while the ventilation system operates during the evening from 20:00 to 22:00.

In Figure 9b, the radiant heating system operates less frequently than in scenario A and avoids operation during peak electricity pricing periods. The ventilation system runs only briefly during the early morning and at 17:00–18:00 in the afternoon, while the dehumidification system remains inactive.

Figure 9c presents the power scheduling under the multi-objective optimization scenario. Compared to scenario A, it reduces the operation time of both radiant heating and dehumidification in certain time periods. Compared to scenario B, it increases dehumidification activity and includes radiant heating during peak load periods, indicating a more balanced approach to economic cost and comfort.

Algorithms 2025, 18, 446 22 of 28

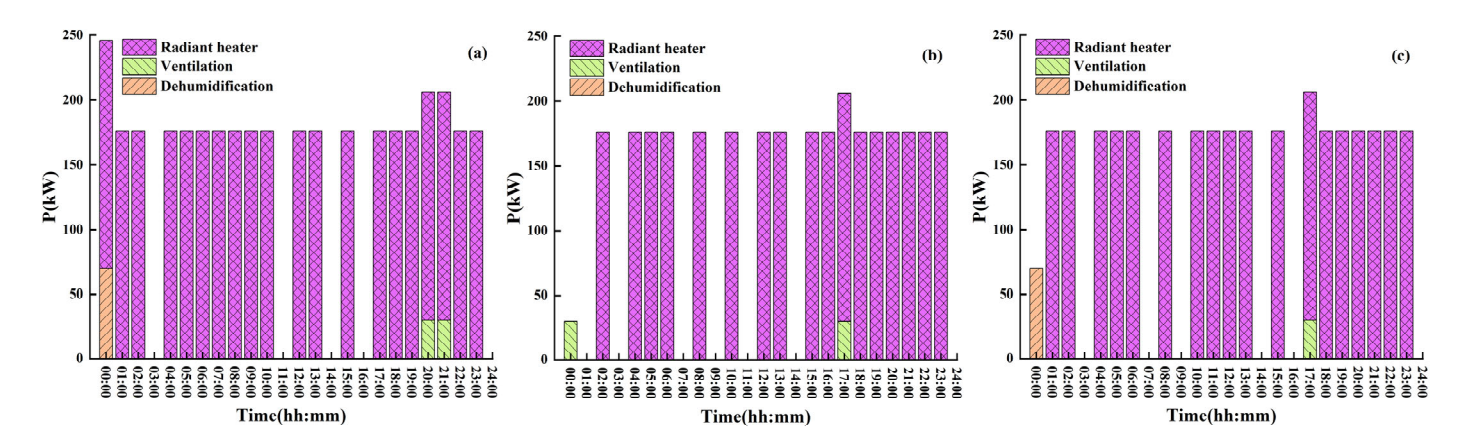


Figure 9. Optimized scheduling results of a typical day in winter: (a) single-objective optimization (F1); (b) single-objective optimization (F2); and (c) multi-objective optimization.

3.3.3. Demand-Side Response Analysis

As shown in Figure 10, multi-objective optimization incurs lower costs under time-of-use electricity pricing compared to fixed-rate pricing under the same comfort level. By incorporating demand-side response and optimizing the scheduling of the climate control system based on dynamic electricity pricing, the operational costs are significantly reduced compared to optimization under fixed pricing. Specifically, the dynamic pricing-based model achieves cost reductions of 25.3% on typical summer days, 24.4% during transitional seasons, and 18.7% on typical winter days. Moreover, the electricity costs are reduced by 27.4%, 25.5%, and 20.6%, respectively. By shifting equipment operation to periods with lower electricity prices, overall costs can be effectively reduced.

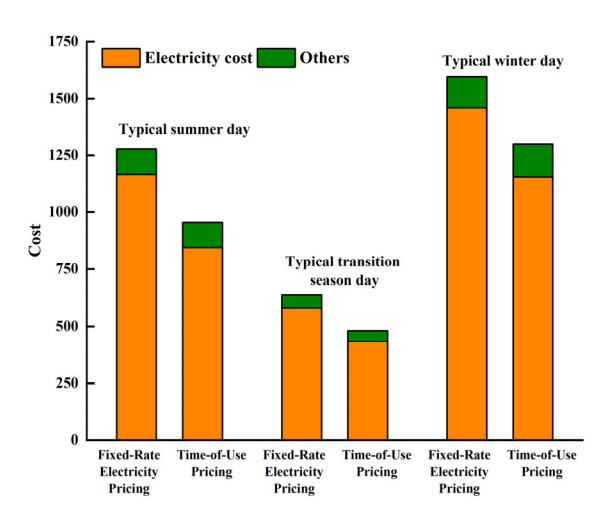


Figure 10. Comparison of electricity cost and other costs under fixed-rate and time-of-use pricing for typical summer, transition season, and winter days.

4. Discussion

In the field of building energy optimization, multi-objective optimization methods have been widely applied to climate control systems in various energy-intensive buildings. Current research primarily focuses on minimizing energy consumption and operational costs while ensuring indoor thermal comfort. With the continuous refinement of energy pricing mechanisms, the integration of demand response strategies has become a research hotspot. In particular, under time-of-use electricity pricing, increasing attention has been paid to the adaptability of optimization models and their capability for precise scheduling. Moreover, an increasing number of optimization studies targeting different types of buildings—such as office buildings, hospitals, residential complexes, and sports

venues—have emerged, providing valuable theoretical foundations and technical references for this study.

This work systematically compared the performance differences in three typical multi-objective optimization algorithms—NSGA-II, MOEA/D, and MOBBO—in the climate control scheduling of ice sports venues. The results show that MOEA/D demonstrates outstanding computational efficiency, making it suitable for scenarios with high time constraints; however, it has certain limitations in solution diversity and convergence. Although the MOBBO algorithm exhibits good search balance and solution coverage, performing well in complex and non-convex problems, its high computational cost limits its practical application. In contrast, NSGA-II delivers the best performance in solution quality, combining strong global search capability with excellent solution diversity, effectively approaching the optimal Pareto front. It is particularly well-suited for scheduling problems that require high solution quality and optimization performance. Considering solution quality, algorithm stability, and practical application needs, NSGA-II was ultimately selected as the core algorithm for climate control optimization in ice sports venues, as it achieved high-quality optimization results and demonstrated the robustness and applicability of the optimization framework.

The multi-objective optimization model can better meet the comprehensive requirements of the climate control system for the operating economy as well as spectator comfort than single-objective optimization. Compared with the model optimized solely for users' comfort, the multi-objective optimization model improves economic performance under typical summer, transitional, and winter conditions by 26.5%, 14.9%, and 15.1%, respectively. In contrast, compared with the cost-optimal model, it reduces spectators' discomfort under the same three typical conditions by 10.0%, 39.3%, and 28.9%, respectively. Furthermore, with the integration of demand response strategies under time-of-use electricity pricing, operational costs are effectively reduced through reasonable load shifting. Operational costs can be significantly reduced by 25.3%, 24.4%, and 18.7% in summer, transitional, and winter conditions, respectively. These results not only verify the optimization capability of the NSGA-II-TOPSIS model but also demonstrate its practical application potential in energy-intensive venues like ice sports arenas, providing a replicable optimization approach and methodological framework for energy scheduling and management in similar settings.

The optimization results of this work exhibit strong consistency with several existing studies. Hosamo et al. proposed a BIM-GLSSVM-NSGA-II framework to optimize both building energy consumption and indoor thermal comfort, which shares similar objectives with this study [53]. Chen focused on minimizing carbon emissions, thermal comfort, and the total comprehensive cost of buildings [54]. Kampelis applied a genetic algorithm combined with demand response strategies to the HVAC system of a nearly zero-energy industrial building to balance daily energy costs and thermal comfort. Through simulations of the Leaf Lab industrial building within the Leaf Community smart microgrid in Marche, Italy, this study reported energy savings ranging from 10.4% to 25%, cost savings ranging from 9.9% to 25%, and a slight reduction in thermal comfort [55]. Xue et al. (2022) conducted a dual-objective optimization of lifecycle cost (LCC) and lifecycle CO2 emissions (LCCO₂) for low-energy residential buildings in severe cold climates during the design phase. Compared with the initial design schemes, the optimized results achieved a reduction of 10.9% to 18.9% in lifecycle cost and a decrease of 13.5% to 22.4% in LCCO₂ [56]. Despite differences in application scenarios, these studies align closely with this research in terms of balancing energy savings and comfort, constructing multi-objective optimization frameworks, and incorporating dynamic electricity pricing response mechanisms, providing strong support for the scientific validity and practical applicability of this work.

Although this work has achieved promising results in the multi-objective optimization scheduling of ice sports venues, several limitations remain. This study considers a specific type of ventilation system and does not account for systems that recover heat from the refrigeration unit. It also does not evaluate the model's performance under uncertain conditions such as weather fluctuations and varying crowd flow. Future research could develop a more comprehensive and detailed ventilation system model that incorporates heat recovery from the refrigeration system. In addition, the impact of multiple uncertainties on spectator zone climate comfort and system operating costs should be further investigated.

5. Conclusions

For the climate control system incorporating ventilation, dehumidification, and radiant heaters, this study developed a multi-objective optimization scheduling model that balances both economic performance and spectator comfort in combination with demand response strategies. The performance of three typical algorithms—NSGA-II, standard MOEA/D, and Multi-Objective Brown Bear Optimization (MOBBO)—was systematically compared. Due to its superior performance in terms of solution diversity and convergence, NSGA-II is adopted to address the problem in this study. The model employs NSGA-II to generate a Pareto solution set and then applies the TOPSIS method to select the optimal solution. Simulation results for summer, winter, and transitional seasons in cold regions show that compared to single-objective optimization approaches that focus solely on either comfort enhancement or cost reduction, the proposed multi-objective model achieves a better balance between user comfort and economic performance.

A two-stage optimization approach combining multi-objective optimization and decision analysis was developed. This method effectively enhances the practicality and operability of the model, providing an efficient and sustainable scheduling optimization solution for climate control systems in energy-intensive buildings such as ice sports venues. It also offers valuable insights for addressing energy management challenges in similar scenarios.

Author Contributions: Conceptualization, Z.D. and Y.L.; methodology, Z.D.; software, Z.D.; validation, Z.D.; formal analysis, Y.X.; writing—original draft preparation, Z.D.; writing—review and editing, B.L.; supervision, B.L.; project administration, Y.L.; funding acquisition, Y.L. All authors have read and agreed to the published version of the manuscript.

Funding: This research is funded by the National Key R&D Program of China, grant number 2023YFE0102100.

Data Availability Statement: The original data presented in this study are openly available on GitHub at https://github.com/Holly616/dataset2.git (accessed on 14 July 2025).

Conflicts of Interest: The authors declare that they have no known competing financial interests or personal relationships that could have appeared to influence the work reported in this paper.

Symbols/Letters

Symbol/ Letters	Description/ Meaning	Symbol/ Letters	Description/ Meaning	Symbol/ Letters	Description/ Meaning
$\theta_z(t)$	ambient temperature of	0	set point temperature	$w_z(t)$	humidity of
	the spectator stands at time t	$\theta_{z,set}$	of the spectator stands		the spectator stands
$w_{z,set}$	set point humidity	7	spectator	C	operational
	of the spectator stands	Z	stands	C_{ECO}	cost
C_{sco}	environmental	$C_{i}(I)$	cost of electricity	$C_{-}(1)$	cost of
	cost	$C_E(t)$	consumption	$C_O(t)$	maintenance

Algorithms **2025**, 18, 446 25 of 28

Symbol/ Letters	Description/ Meaning	Symbol/ Letters	Description/ Meaning	Symbol/ Letters	Description/ Meaning
$C_S(t)$	cost of startup and	τ	time	$C_E^{ven}(t)$	electricity costs of
$C_E^{dh}(t)$	shutdown of machine electricity costs of dehumidification	$C_E^{ht}(t)$	interval electricity costs of radiant heating	$C_{OM}^{ven}(t)$	ventilation system maintenance costs of ventilation system
$C_{OM}^{dh}(t)$	maintenance costs of dehumidification	$C_{OM}^{ht}(t)$	maintenance costs of radiant heating	$C^{ven}_{SC}(t)$	startup and shutdown costs of ventilation system
$C^{dh}_{SC}(t)$	startup and shutdown costs of dehumidification	$C^{ht}_{SC}(t)$	startup and shutdown costs of radiant heating	Qven	cooling load provided by the ventilation system
COP	coefficient of performance of the ventilation system	P_{dh}	power of dehumidifier	P_{ven}	power of ventilation system
$S_{ven}(t)$	binary variables of ventilation system power of	$S_{ht}(t)$	binary variables of radia-tion heaters cost coefficient of	$S_{dh}(t)$	binary variables of dehumidifier
P_{ht}	radiation heaters	$C_{om-dh}(t)$	mainte-nance of dehumidifier	$C_{ele}(t)$	electricity price
$C_{om-ven}(t)$	cost coefficient of maintenance of ventilation	$C_{sc-dh}(t)$	cost coefficient of startup and shutdown of dehumidifier	$C_{om-ht}(t)$	cost coefficient of maintenance of radiation heaters
$C_{sc-ven}(t)$	cost coefficient of startup and shutdown of machine of ventilation	C_{co2}	environmental cost of carbon emissions from electricity	$C_{sc-ht}(t)$	cost coefficient of startup and shutdown of radiation heaters
EF	carbon emission factors for electricity maximum	P_{atm}	atmospheric pressure lower	$w_z(t)$	humidity at time <i>t</i> intermediate coefficient of
\varnothing_z^{max}	relative humidity	$ heta_z^l$	limit of the	$ez_{s(t)}$	conversion of temperature, relative humidity and
	setpoint temperature		temperature the impact of the		specific humidity upper limit
$\theta_z(t)$	at time t	$w_{ven}(t)$	ventilation system on the humidity	θ_z^u	of the temperature
$w_z(t-1)$	air humidity in the ice sports venue at time $t-1$	$w_{dh}(t)$	effect of dehumidifier operation on the humidity	$w_{leak}(t)$	the effect of air infiltration on the humidity
$w_{aud}(t)$	the moisture generated by audience respiration	V_z	volume of air in the Z area (m ³)	\dot{V}	airflow rate of the ventilation system (m ³ /h)
$w_{ex}(t)$	humidity of the incoming air (kg _{H2O} /kg _{air}) the intermediate coefficient	$\theta_{ex}(t)$	temperature of the outside air at time <i>t</i> (K) the total	$\varnothing_{ex}(t)$	relative humidity of the outside air at time t (%)
$ex_{s(t)}$	of conversion of temperature , relative humidity and specific humidity outside	N	capacity of the ice sports venue(persons)	V_z^{leak}	air leakage (m^3/h)
$N_s(t)$	occupancy rate of the venue (%)	ρ	air density (kg _{air} /m³)	φ	the clustering coefficient
8	hourly moisture emission per person (kg/h) ambient	$\theta_z(t-1)$	ambient temperature at time $t - 1$ (K) the effect of ventilation	$v_Z(t)$	the impact of dehumidifier operation on the moisture content of the air (kg/h) the effect of
$\theta_z(t)$	temperature at time <i>t</i> (K) effect of outdoor air heat	$\theta_{ven}(t)$	system operation on temperature (K) effect of ice temperature	$\theta_{ht}(t)$	radiant heating on temperature (K) the effect
$\theta_{en}(t)$	conduction through the envelope on temperature (K)	$\theta_{ref}(t)$	through thermal radiation on temperature (K)	$\theta_{light}(t)$	of lighting on temperature (K)

Algorithms 2025, 18, 446 26 of 28

Symbol/	Description/	Symbol/	Description/	Symbol/	Description/
Letters	Meaning	Letters	Meaning	Letters	Meaning
	effect of body heat		air		mass of the air
$\theta_{aud}(t)$	dissipation on	ρ	density	m_z	in the spectator
	temperature (K)		(kg/m^3)		stands (kg)
	specific heat capacity		air leakage		heat transfer coefficient of
C_Z	of air	m	flow rate	U	the building envelope
	$(1.005 kJ/(kg\cdot K))$		(m^3/h)		$(kW/(m^2\cdot K))$
A	surface area of the	<u>.</u> .	air mass flow	D	total power of the light in
A	building envelope (m²)	\dot{v}	rate (kg/h)	P_{light}	the spectator stands (kW)
oven	setpoint temperature for	NI (4)	schedule of audience occupancy	NI	maximum capacity of
θ_z^{ven}	ventilation system	$N_{aud}(t)$	as a percentage (%)	N_{max}	the audience (Person)
	heat generated by indoor	0	radiative heat of the	0	radiative heat of the
9rad	occupants (W/(h·Person))	Q_y	surfaces in zones Y	Q_z	surfaces in zones Z
0	radiative heat of the	Δ	contact area between zones	Г	shape factor between
Q_x	surfaces in zones X	$A_{y,z}$	Y and $Z(m^2)$	$F_{x,z}$	zones X and Z
Λ	contact area between	C	emissivity	σ	proportional constant
$A_{x,z}$	zones X and $Z(m^2)$	ϵ	coefficient		(kW/m^2)
	shape factor		width of the vertical		width of the
$F_{y,z}$	between zones	$w_{x,z}$	plane of the contact surface	$l_{x,z}$	X and Z
	Y and Z		between zones X and Z		contact surface
	temperature of		width of the vertical		width of the
$\theta_{x}(t)$	zone X at	$w_{y,z}$	plane of the contact surface	$l_{y,z}$	Y and Z
	time t (K)		between zones Y and Z		contact surface
1.	height of the X and	14	height of the Y and		
$h_{x,z}$	Z contact surface	$h_{y,z}$	Z contact surface		

References

- 1. International Ice Hockey Federation. IIHF Ice Rink Guide 2016; International Ice Hockey Federation: Zurich, Switzerland, 2016.
- 2. Palmowska, A.; Lipska, B. Experimental study and numerical prediction of thermal and humidity conditions in the ventilated ice rink arena. *Build. Environ.* **2016**, *108*, 171–182. [CrossRef]
- 3. Lin, W.; Liu, X.; Tao, Z. Experimental and numerical study of zonal heat and moisture migration inside artificial ice rinks. *Build. Environ.* **2023**, 245, 110897. [CrossRef]
- 4. Gu, M.; Guo, Q.; Lu, S. Feasibility analysis of energy-saving potential of the underground ice rink using spectrum splitting sunshade technology. *Renew. Energy* **2022**, *191*, 571–579. [CrossRef]
- 5. Lind, P. A Study of Modelling the Energy System of an Ice Rink Sports Facility: Modelling the Heating and Cooling of ABB Arena Syd and Implementation of Renewable Energy Sources Using TRNSYS. Master's Thesis, Mälardalen University, Västerås, Sweden, 2018.
- 6. Lair, L. Design of a Net-Zero Carbon Ice Hockey Rink with Renewable Energy. Master's Thesis, California State University, Long Beach, CA, USA, 2021.
- 7. Wei, Z.; Liu, D. On Design of Low-Operation-Cost Ice Arenas with Energy Saving Approaches. *Procedia Eng.* **2016**, 169, 38–43. [CrossRef]
- 8. Deori, L.; Giulioni, L.; Prandini, M. Optimal building climate control: A solution based on nested dynamic programming and randomized optimization. In Proceedings of the 53rd IEEE Conference on Decision and Control, Los Angeles, CA, USA, 15–17 December 2014; pp. 4905–4910. [CrossRef]
- 9. Jain, R. Optimal Operation of Climate Control Systems of Indoor Ice Rinks. Master's Thesis, University of Waterloo, Waterloo, ON, Canada, 2013.
- 10. Zhang, T.; Wan, M.P.; Ng, B.F.; Yang, S. Model predictive control for building energy reduction and temperature regulation. In Proceedings of the 2018 IEEE Green Technologies Conference (GreenTech), Austin, TX, USA, 4–6 April 2018. [CrossRef]
- 11. Bozchalui, M.C.; Hashmi, S.A.; Hassen, H.; Canizares, C.A.; Bhattacharya, K. Optimal operation of residential energy hubs in smart grids. *IEEE Trans. Smart Grid* **2012**, *3*, 1755–1766. [CrossRef]

12. Zahedi, R.; Omidifar, R.; Balaghi, S.F.; Pourezzat, A.A.; Yousefi, H.; Taghitahooneh, M.; Shaghaghi, A.; Ahmadi, A. Heating, cooling and energy management of cold climate educational built environments using green roofs. *Urban Gov.* **2024**, *4*, 297–312. [CrossRef]

- 13. Li, W.; Xu, P. A fast method to predict the demand response peak load reductions of commercial buildings. *Sci. Technol. Built Environ.* **2016**, 22, 633–642. [CrossRef]
- 14. McKenna, E.; Thomson, M. Demand response behavior of domestic consumers with photovoltaic systems in the UK: An exploratory analysis of an internet discussion forum. *Energy Sustain. Soc.* **2014**, *4*, 13. [CrossRef]
- 15. Vand, B.; Lopes, Y.K.; Hathway, E.A.; Rockett, P. Sensitivity analysis of building physical parameters to maximize heating energy saving using MPC. In Proceedings of the 3rd International Conference on Energy Harvesting, Storage, and Transfer, Ottawa, ON, Canada, 18–19 June 2019. [CrossRef]
- 16. Vand, B.; Martin, K.; Jokisalo, J.; Kosonen, R.; Hast, A. Demand response potential of district heating and ventilation in an educational office building. *Sci. Technol. Built Environ.* **2019**, *26*, 304–319. [CrossRef]
- 17. Claessens, B.J.; Vanhoudt, D.; Desmedt, J.; Ruelens, F. Model-free control of thermostatically controlled loads connected to a district heating network. *Energy Build.* **2018**, *159*, 1–10. [CrossRef]
- 18. Zahedi, R.; Shaghaghi, A.; Aslani, A.; Noorollahi, Y.; Astaraei, F.R.; Eskandarpanah, R. Optimization of a hybrid cooling, heating and power multigeneration system coupled with heat storage tank using a developed algorithm. *J. Therm. Anal. Calorim.* **2024**, 149, 11107–11117. [CrossRef]
- 19. Široký, J.; Oldewurtel, F.; Cigler, J.; Prívara, S. Experimental analysis of model predictive control for an energy efficient building heating system. *Appl. Energy* **2011**, *88*, 3079–3087. [CrossRef]
- 20. Gwerder, M.; Jürg, T. Predictive control for integrated room automation. In Proceedings of the 8th REHVA World Congress Clima, Lausanne, Switzerland, 9–12 October 2005.
- 21. Nagpal, H.; Biswajit, B.; Andrea, S. Economic model predictive control of building energy systems in cooperative optimization framework. In Proceedings of the 2018 Indian Control Conference (ICC), Kanpur, India, 4–6 January 2018. [CrossRef]
- 22. Imandoust, M.; Alghorayshi, S.T.K.; Javidfar, M.; Asadi, B.; Jafarinasab, M.; Qezelbigloo, S.; Zahedi, R. Technical-economic analysis and optimization of multiple effect distillation system by solar energy conversion as the heat source. *Appl. Energy* **2024**, 280, 112859. [CrossRef]
- 23. Zhang, Q.; Li, H. MOEA/D: A multi objective evolutionary algorithm based on decomposition. *IEEE Trans. Evol. Comput.* **2007**, 11, 712–731. [CrossRef]
- 24. Deb, K.; Pratap, A.; Agarwal, S.; Meyarivan, T. A fast and elitist multi-objective genetic algorithm: NSGA-II. *IEEE Trans. Evol. Comput.* **2002**, *6*, 182–197. [CrossRef]
- 25. Mehta, P.; Kumar, S.; Tejani, G.G.; Khishe, M. MOBBO: A multi-objective brown bear optimization algorithm for solving constrained structural optimization problems. *J. Optim.* **2024**, 2024, 5546940. [CrossRef]
- 26. Behzadian, M.; Kazemzadeh, R.B.; Albadvi, A.; Aghdasi, M. A state-of-the-art survey of TOPSIS applications. *Expert Syst. Appl.* **2012**, *39*, 13051–13069. [CrossRef]
- Hemati, P.; Montagud-Montalvá, C.I.; Sawalha, S. Comparative Analysis of Modern Energy Systems for Ice Rinks. Master's Thesis, Energy Technologies for Sustainable Development, Valencia, Spain, September 2023.
- 28. Olama, M.M.; Kuruganti, T.; Nutaro, J.; Dong, J. Coordination and control of building HVAC systems to provide frequency regulation to the electric grid. *Energies* **2018**, *11*, 1852. [CrossRef]
- 29. Fratean, A.; Dobra, P. Key performance indicators for the evaluation of building indoor air temperature control in a context of demand side management: An extensive analysis for Romania. *Sustain. Cities Soc.* **2021**, *68*, 102805. [CrossRef]
- 30. Kang, J.; Weng, S.; Li, Y.; Ma, T. Study of Building Demand Response Method Based on Indoor Temperature Setpoint Control of VRV Air Conditioning. *Buildings* **2022**, *12*, 415. [CrossRef]
- 31. Alıç, O.; Filik, Ü.B. A multi-objective home energy management system for explicit cost-comfort analysis considering appliance category-based discomfort models and demand response programs. *Energy Build.* **2021**, 240, 110868. [CrossRef]
- 32. Imandoust, M.; Alghorayshi, S.T.K.; Asadi, B.; Montazeri, A.; Moradi, F.; Zahedi, R. Optimizing solarized desalination unit through the implementation of 4-step MED method using energy, exergy, economic and environmental analysis. *J. Environ. Manag.* **2024**, *370*, 122707. [CrossRef] [PubMed]
- 33. Munankarmi, P.; Maguire, J.; Balamurugan, S.P.; Blonsky, M.; Roberts, D.; Jin, X. Community-scale interaction of energy efficiency and demand flexibility in residential buildings. *Appl. Energy* **2021**, 298, 117149. [CrossRef]
- 34. Golpîra, H.; Syed, A.R.K. A multi-objective risk-based robust optimization approach to energy management in smart residential buildings under combined demand and supply uncertainty. *Energy* **2019**, *170*, 1113–1129. [CrossRef]
- 35. Vahidinasab, V.; Jadid, S. Multi-objective environmental/techno-economic approach for strategic bidding in energy markets. *Appl. Energy* **2009**, *86*, 496–504. [CrossRef]
- 36. Wong, S.; Kankar, B.; David, F.J. Long-term effects of feed-in tariffs and carbon taxes on distribution systems. *IEEE Trans. Power Syst.* **2010**, 25, 1241–1253. [CrossRef]

Algorithms 2025, 18, 446 28 of 28

37. Johansson, B. Climate policy instruments and industry—Effects and potential responses in the Swedish context. *Energy Policy* **2006**, *34*, 2344–2360. [CrossRef]

- 38. Government of British Columbia. *Tax Cuts*; Funded by a Revenue Neutral Carbon Tax; Government of British Columbia: Victoria, BC, Canada, 2009.
- 39. Wang, J.; Guo, Z.; Ye, Q.; Gao, D. An LSTM Forest fire prediction model based on buffer resampling. *China Safety Sci. Technol.* **2023**, *19*, 195–202. (In Chinese)
- 40. Hakan, C.A.; Arif, H.B. Energy and exergy analyses of ice rink buildings at varying reference temperatures. *Energy Build.* **2010**, 42, 1418–1425. [CrossRef]
- 41. Taebnia, M.; Toomla, S.; Leppä, L.; Kurnitski, J. Developing energy calculation methodology and calculation tool validations: Application in air-heated ice rink arenas. *Energy Build.* **2020**, 226, 110389. [CrossRef]
- 42. Acerce, A.; Denizhan, B. Application of the Non-Dominated Sorting Genetic Algorithm II (NSGA-II) in a Two-Echelon Cold Supply Chain. *Systems* **2025**, *13*, 206. [CrossRef]
- 43. Fan, Q.; Han, Y.; Zhang, A.; Bi, W. Numerical Design Structure Matrix–Genetic Algorithm-Based Optimization Method for Design Process of Complex Civil Aircraft Systems. *Systems* **2024**, *12*, 566. [CrossRef]
- 44. Wan, M.; Qu, T.; Huang, G.Q.; Chen, R.; Huang, M.; Pan, Y.; Nie, D.; Chen, J. A Bi-Objective Model for the Location and Optimization Configuration of Kitchen Waste Transfer Stations. *Systems* **2024**, *12*, 571. [CrossRef]
- 45. Zhang, Q.; Si, H.; Qin, J.; Duan, J.; Zhou, Y.; Shi, H.; Nie, L. Double Deep Q-Network-Based Solution to a Dynamic, Energy-Efficient Hybrid Flow Shop Scheduling System with the Transport Process. *Systems* **2025**, *13*, 170. [CrossRef]
- 46. Nuh, J.A.; Koh, T.W.; Baharom, S.; Osman, M.H.; Kew, S.N. Performance Evaluation Metrics for Multi-Objective Evolutionary Algorithms in Search-Based Software Engineering: Systematic Literature Review. *Appl. Sci* **2021**, *11*, 3117. [CrossRef]
- 47. Kalita, K.; Chohan, J.S.; Jangir, P.; Chakraborty, S. A new decomposition-based multi-objective symbiotic organism search algorithm for solving truss optimization problems. *Decis. Anal. J.* **2024**, *10*, 100371. [CrossRef]
- 48. Zhang, S.; Esangbedo, M.O. Urban Scenic Spot Activity Center Investment: Strategic Construction Company Selection Using the Grey System-II Thinking Compromise Ranking of Alternatives from Distance to Ideal Solution Multi-Criteria Decision-Making Method. Systems 2025, 13, 67. [CrossRef]
- 49. Klarić, K.; Perić, I.; Vukman, K.; Papić, F.; Klarić, M.; Grošelj, P. Hybrid MCDM-FMEA Model for Process Optimization: A Case Study in Furniture Manufacturing. *Systems* **2025**, *13*, 14. [CrossRef]
- 50. Yang, W.; Wu, Y. A Novel TOPSIS Method Based on Improved Grey Relational Analysis for Mult attribute Decision-Making Problem. *Math. Probl. Eng.* **2019**, 2019, 8761681. [CrossRef]
- 51. Lou, Y.; Ye, Y.; Yang, Y.; Zuo, W. Long-term carbon emission reduction potential of building retrofits with dynamically changing electricity emission factors. *Build. Environ.* **2022**, *210*, 108683. [CrossRef]
- 52. Bi, Y.; Lin, Y.; Qin, L.; Wang, H.; Sun, R. Performance optimization of a solar air-conditioning with a three-phase accumulator based on the energy-economic analysis. *J. Build. Eng.* **2022**, *59*, 105065. [CrossRef]
- 53. Hosamo, H.H.; Tingstveit, M.S.; Nielsen, H.K.; Svennevig, P.R.; Svidt, K. Multi objective optimization of building energy consumption and thermal comfort based on integrated BIM framework with machine learning-NSGA II. *Energy Build.* 2022, 277, 112479. [CrossRef]
- 54. Chen, R.; Tsay, Y.-S.; Ni, S. An integrated framework for multi-objective optimization of building performance: Carbon emissions, thermal comfort, and global cost. *J. Clean. Prod.* **2022**, *359*, 131978. [CrossRef]
- 55. Kampelis, N.; Sifakis, N.; Kolokotsa, D.; Gobakis, K.; Kalaitzakis, K.; Isidori, D.; Cristalli, C. HVAC Optimization Genetic Algorithm for Industrial Near-Zero-Energy Building Demand Response. *Energies* **2019**, *12*, 2177. [CrossRef]
- 56. Xue, Q.; Wang, Z.; Chen, Q. Multi-Objective Optimization of Building Design for Life Cycle Cost and CO₂ Emissions: A Case Study of a Low-Energy Residential Building in a Severe Cold Climate. *Build. Simul.* **2022**, *15*, 83–98. [CrossRef]

Disclaimer/Publisher's Note: The statements, opinions and data contained in all publications are solely those of the individual author(s) and contributor(s) and not of MDPI and/or the editor(s). MDPI and/or the editor(s) disclaim responsibility for any injury to people or property resulting from any ideas, methods, instructions or products referred to in the content.